

Chapter 9

A Hybrid Scheme for Two-Phase Flow

In this chapter, we investigate a two-phase flow generalization of the Euler equations. A stochastic two-phase problem in one spatial dimension is investigated as a first step towards developing an intrusive method for complex multiphysics problems, such as shock-bubble interactions, high-speed reacting flows with liquid fuels, and Richtmyer-Meshkov instability, with generic with generic uncertainty in the input parameters. So et al. [20] investigated a two-dimensional two-phase problem subject to uncertainty in bubble deformation and contamination of the gas bubble, based on the experiments in [10]. The eccentricity of the elliptic bubble and the ratio of air-helium of the bubble were assumed to be random variables, and quantities of interest were obtained by numerical integration in the stochastic range (stochastic collocation). Previous work on uncertainty quantification for multiphase problems include petroleum reservoir simulations with stochastic point collocation where deterministic flow solvers are evaluated at stochastic collocation points [14] and Karhunen-Loève (KL) expansions combined with perturbation methods [3]. This chapter is based on the work in [17].

We assume uncertainty in the location of the material interface, which requires a stochastic representation of all flow variables. Stochastic quantities are represented as a generalized chaos series, that could be either global as in the case of generalized polynomial chaos [24], or localized (see e.g. [5]). For robustness, we use a generalized chaos expansion with multiwavelets to represent the solution in the stochastic dimension [18]. Note that this basis is global, so the method is fully intrusive. However, the basis is hierarchically localized in the sense that multiwavelets belonging to the same resolution level are grouped into families with non-overlapping support. These features make it suitable for approximating discontinuities in the stochastic space without the oscillations that occur in global polynomial bases.

The stochastic Galerkin method is applied to the stochastic two-phase formulation, resulting in a finite-dimensional deterministic system that shares many

properties with the original deterministic problem. The regularity properties of the stochastic problem are essential in the design of an appropriate numerical method. Chen et al. studied the steady-state inviscid Burgers' equation with a source term [4]. We used a similar approach for the inviscid Burgers' equation with uncertain boundary conditions and also analyzed the regularity of low-order stochastic Galerkin approximations of the problem [16]. Schwab and Tokareva analyzed regularity of scalar hyperbolic conservation laws and a linearized version of the Euler equations with uncertain initial profile [19]. In this chapter, we analyze smoothness of the stochastic two-phase problem.

The stochastic Galerkin problem is hyperbolic. This generalized and extended two-phase problem is solved with a hybrid method coupling the continuous phase region with the discontinuous phase region through a numerical interface. The non-smooth region is solved with the HLL-flux, MUSCL-reconstruction in space, and fourth-order Runge-Kutta integration in time. The minmod flux limiter is employed in the experimental results displayed below.

Finite-difference operators in summation-by-parts (SBP) form are used for the high-order spatial discretization. A symmetrized problem formulation that generalizes the energy estimates in [8] for the Euler equations is used for the stochastic Galerkin system. The coupling between the different solution regions is performed with a weak imposition of the interface conditions through an interface using a penalty technique [2]. A fourth-order Runge-Kutta method is used for the integration in time.

9.1 Two-Phase Flow Problem

We assume two phases with volume fractions α and $\beta = 1 - \alpha$ on the domain $x \in [0, 1]$, governed by the advection equation

$$\frac{\partial}{\partial t}\alpha + v'(x, t)\frac{\partial}{\partial x}\alpha = 0, \quad (9.1)$$

where we let $v'(x, t) = v(x, t)$ be the advective velocity obtained from the conservative Euler system below. The Euler equations determine the conservation of masses $\alpha\rho_\alpha$ and $\beta\rho_\beta$, momentum ρv , and total energy E of the two phases through

$$\frac{\partial \mathbf{u}}{\partial t} + \frac{\partial \mathbf{f}}{\partial x} = 0, \quad (9.2)$$

where

$$\mathbf{u} = \begin{bmatrix} \alpha\rho_\alpha \\ \beta\rho_\beta \\ \rho v \\ E \end{bmatrix}, \quad \mathbf{f} = \begin{bmatrix} \alpha\rho_\alpha v \\ \beta\rho_\beta v \\ \rho v^2 + p \\ (E + p)v \end{bmatrix}. \quad (9.3)$$

We assume that the pressure p is given by the perfect gas equation of state for two phases

$$p = (\gamma - 1) \left(E - \frac{1}{2} \rho v^2 \right), \quad \gamma = \frac{1}{\frac{\alpha}{\gamma_\alpha} + \frac{\beta}{\gamma_\beta}},$$

where γ is the weighted ratio of specific heats. The total density is given by $\rho = \alpha \rho_\alpha + \beta \rho_\beta$. Note that the sum of the first and second equations of (9.2) is the standard mass conservation of the Euler equations. Thus, an equivalent formulation is the Euler equations supplemented with an extra mass conservation equation for one of the phases α and β .

We investigate the Riemann problem defined by the initial conditions

$$(\alpha, \alpha \rho_\alpha, \beta \rho_\beta, \rho v, E)^T = \begin{cases} (1, 1, 0, 0, 2.5)^T & x < x_0 + \xi \\ (0, 0, 0.125, 0, 0.25)^T & x > x_0 + \xi \end{cases}, \quad (9.4)$$

where ξ is a parametrization of the measured or modeled uncertainty in the initial membrane location. Despite the seemingly simple nature of the initial condition, the MW series of the initial condition has an infinite number of nonzero terms. Thus, stochastic truncation error is an issue already at $t = 0$.

The stochastic Galerkin formulation of the two-phase problem is obtained by multiplying (9.1) and (9.2) by each one of the basis functions $\psi_i(\xi)$, and integrating with respect to the probability measure \mathcal{P} over the range of ξ . Initial functions are obtained by projection of (9.4) onto the basis functions $\psi_i(\xi)$. The MW expansion is truncated to $M + 1$ terms and we get the systems for the MW coefficients

$$\frac{\partial}{\partial t} \alpha_k + \sum_{i=0}^M \sum_{j=0}^M v_i \frac{\partial}{\partial x} \alpha_j \langle \psi_i \psi_j \psi_k \rangle = 0, \quad k = 0, \dots, M, \quad (9.5)$$

$$\beta_k = \delta_{k0} - \alpha_k, \quad k = 0, \dots, M, \quad (9.6)$$

and

$$\frac{\partial}{\partial t} \begin{bmatrix} (\alpha \rho_\alpha)_k \\ (\beta \rho_\beta)_k \\ (\rho v)_k \\ E_k \end{bmatrix} + \frac{\partial}{\partial x} \begin{bmatrix} \sum_{i=0}^M \sum_{j=0}^M (\alpha \rho_\alpha)_i v_j \langle \psi_i \psi_j \psi_k \rangle \\ \sum_{i=0}^M \sum_{j=0}^M (\beta \rho_\beta)_i v_j \langle \psi_i \psi_j \psi_k \rangle \\ \sum_{i=0}^M \sum_{j=0}^M (\rho v)_i v_j \langle \psi_i \psi_j \psi_k \rangle + p_k \\ \sum_{i=0}^M \sum_{j=0}^M (E_i + p_i) v_j \langle \psi_i \psi_j \psi_k \rangle \end{bmatrix} = 0, \quad k = 0, \dots, M. \quad (9.7)$$

MW expansions for pressure can be updated from the MW of the conservative variables, and then be inserted into the fluxes. It is not possible in general to find a Roe-like variable transformation as was done for the single-phase Euler equations in Chap. 8. We use a pseudospectral approximation of high-order stochastic products for the pressure update. In the computation of, for example, the order M product

$z(\xi) = \sum_{k=0}^M z_k \psi_k$ of three stochastic variables $a(\xi)$, $b(\xi)$, $c(\xi)$, for $k = 0, \dots, M$, we use the approximation

$$\begin{aligned} z_k &= (a(\xi)b(\xi)c(\xi))_k = \left\langle \left(\sum_{i=0}^M a_i \psi_i(\xi) \right) \left(\sum_{j=0}^M b_j \psi_j(\xi) \right) \left(\sum_{l=0}^M c_l \psi_l(\xi) \right) \psi_k(\xi) \right\rangle \\ &= \sum_{i=0}^M \sum_{j=0}^M \sum_{l=0}^M \langle \psi_i \psi_j \psi_k \psi_l \rangle a_i b_j c_l \approx \sum_{i=0}^M \sum_{m=0}^M \langle \psi_i \psi_m \psi_k \rangle a_i \underbrace{\sum_{j=0}^M \sum_{l=0}^M \langle \psi_j \psi_l \psi_m \rangle b_j c_l}_{(bc)_m^M} \\ &\equiv (a * (b * c))_k, \end{aligned} \quad (9.8)$$

where the pseudospectral product $y = a * b$ of order M is defined by

$$y_k^M = (a * b)_k = \sum_{i=0}^M \sum_{j=0}^M \langle \psi_i \psi_j \psi_k \rangle a_i b_j, \quad k = 0, \dots, M. \quad (9.9)$$

In matrix notation, we can express (9.9) as

$$\mathbf{y}^M = \mathbf{A}(\mathbf{a}^M)\mathbf{b}^M, \quad (9.10)$$

where $\mathbf{y}^M = (y_0, \dots, y_M)^T$ is the vector of MW coefficients of y and

$$[\mathbf{A}(\mathbf{a}^M)]_{j+1,k+1} = \sum_{i=0}^M \langle \psi_i \psi_j \psi_k \rangle a_i. \quad (9.11)$$

By successively applying (9.10), we obtain approximations of a range of stochastic functions including polynomials, square roots and inverse quantities [6].

For general stochastic basis functions and general choices of the order of generalized chaos, the stochastic volume fractions α and β cannot be guaranteed to be non-negative. In fact, using first-order Legendre polynomial chaos and projecting the initial condition results in $\alpha(x, t = 0, \xi) = \alpha_0(x, t = 0) + \alpha_1(x, t = 0)\xi$, $\xi \in \mathcal{U}[-1, 1]$. This implies that $\alpha(x, t, \xi) < 0$ for some values of x, t, ξ , which is clearly undesirable. However, we only use Legendre polynomials for the convergence test of a smooth problem using the method of manufactured solutions in Sect. 9.4.1. For the fully discontinuous problem, we use Haar wavelets (piecewise constant multiwavelets, $N_p = 0$) for which the initial function always is physical, no matter the order of wavelet expansion. To see this, we rewrite the stochastic advection system (9.5) in matrix-vector notation,

$$\frac{\partial}{\partial t} \boldsymbol{\alpha}^M + \mathbf{A}(\mathbf{v}^M(x, t)) \frac{\partial}{\partial x} \boldsymbol{\alpha}^M = 0,$$

where $\mathbf{A}(\cdot)$ is defined by (9.11). Assuming Haar wavelets, the matrix $\mathbf{A}(\mathbf{v}^M(x, t))$ in the stochastic advection system can be diagonalized with constant eigenvectors y_k , but space- and time-dependent eigenvalues $\lambda_k(x, t)$, for $k = 0, \dots, M$. The stochastic Galerkin advection problem then decouples to a set of scalar advection problems,

$$\frac{\partial}{\partial t} \tilde{\alpha}_k + \lambda_k(x, t) \frac{\partial}{\partial x} \tilde{\alpha}_k = 0, \quad \tilde{\alpha}(x, t = 0) = \tilde{\alpha}_k^{init}(x), \quad k = 0, \dots, M, \quad (9.12)$$

where $\tilde{\alpha}_k = y_k^T \alpha$. The solution of the semilinear advection problem (9.12) is $\tilde{\alpha}_k^{init}(r_k(x, t))$ where r_k is defined by $t = \int_{r_k}^x \frac{dx'}{\lambda_k(x', t)}$. No matter the exact form of r_k , the solution will never attain values beyond the range of $\tilde{\alpha}_k^{init}$. This implies that the stochastic volume fraction PDE formulation will never yield unphysical values.

9.2 Smoothness Properties of the Solution

9.2.1 Analytical Solution

The exact solutions to (9.1) and (9.2) subject to (9.4) can be determined analytically, and are discontinuous for all times. The advection problem (9.1) with v independent of x and t has the solution

$$\alpha(x, t) = \alpha_0(x - vt),$$

which is to be interpreted in the weak sense here since it is discontinuous for all t when α_0 is chosen to be a step function. The conservation law (9.2) is a straightforward extension of the Sod test case for shock tube problems, and its exact piecewise smooth solution can be found in [21]. The solution consists of five distinct smooth regions (denoted $\mathbf{u}_{(L)}$, $\mathbf{u}_{(exp)}$, $\mathbf{u}_{(2)}$, $\mathbf{u}_{(1)}$, and $\mathbf{u}_{(R)}$), and the discontinuities may be found at the interfaces between the different regions. Assume that the initial interface location is $x_0^s = x_0 + \xi$ as given in (9.4). We can then express the deterministic solution for any fixed ξ as a piecewise smooth solution, separated by the four spatial points

$$x_1(t, \xi) = x_0 + \xi - \sqrt{\gamma \frac{p_L}{\rho_L}} t \quad (9.13)$$

$$x_2(t, \xi) = x_0 + \xi + \left(v_2 - \sqrt{\gamma \frac{p_2}{\rho_2}} \right) t \quad (9.14)$$

$$x_3(t, \xi) = x_0 + \xi + v_2 t \quad (9.15)$$

$$x_4(t, \xi) = x_0 + \xi + M_s t, \quad (9.16)$$

where M_s is the Mach number of the shock.

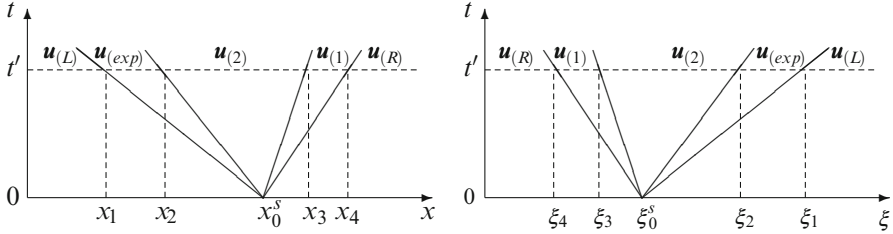


Fig. 9.1 Schematic representation of the solution of the two-phase problem. Solution regions in the $x - t$ space for a fixed ξ (left), and solution regions in $\xi - t$ space for a fixed x (right)

Any given value of ξ will determine the location of the different regions of piecewise continuous solutions, so the true stochastic solution can be expressed as a function of ξ and the variables of the true deterministic solution. In the x - t - ξ -space, all solution discontinuities are defined by triplets (x, t, ξ) satisfying (9.13)–(9.16). The solution regions are depicted in Fig. 9.1 (left) for any fixed value of ξ .

For any point x , the solution regions can be defined as functions of ξ and t . This is shown in Fig. 9.1 (right), where the points in the stochastic dimension separating the different solution regions are given by

$$\xi_1(x, t) = x - x_0 + \sqrt{\gamma \frac{\rho_L}{\rho_L}} t \quad (9.17)$$

$$\xi_2(x, t) = x - x_0 - \left(v_2 - \sqrt{\gamma \frac{\rho_2}{\rho_2}} \right) t \quad (9.18)$$

$$\xi_3(x, t) = x - x_0 - v_2 t \quad (9.19)$$

$$\xi_4(x, t) = x - x_0 - M_s t. \quad (9.20)$$

The solution can be written

$$\begin{aligned} \mathbf{u}(x, t, \xi) = & \mathbf{u}_{(L)} \mathbb{1}_{\{\xi_1 < \xi\}} + \mathbf{u}_{(exp)}(x - \xi) \mathbb{1}_{\{\xi_2 < \xi \leq \xi_1\}} + \mathbf{u}_{(2)} \mathbb{1}_{\{\xi_3 < \xi \leq \xi_2\}} \\ & + \mathbf{u}_{(1)} \mathbb{1}_{\{\xi_4 < \xi \leq \xi_3\}} + \mathbf{u}_{(R)} \mathbb{1}_{\{\xi \leq \xi_4\}}, \end{aligned} \quad (9.21)$$

where the indicator function $\mathbb{1}_{\{A\}}$ of a set A is defined by $\mathbb{1}_{\{A\}}(\xi) = 1$ if $\xi \in A$ and zero otherwise.

Note that if the range of ξ is bounded, some solution states may not occur with nonzero probability for an arbitrary x . The situation shown in Fig. 9.1 (right) requires a sufficiently large range of ξ , or, equivalently, that x is sufficiently close to x_0 . The expression (9.21) is always true, however.

9.2.2 Stochastic Modes

The solutions of (9.1) and (9.2) for fixed values of ξ are discontinuous, but the stochastic modes (multiwavelet coefficients) are continuous. To see this, we proceed from the solution (9.21) to derive exact expressions for the stochastic modes. We assume that the probability measure \mathcal{P} has a probability density \tilde{p} . The k th mode \mathbf{u}_k is given by the projection of (9.21) on $\psi_k(\xi)$,

$$\begin{aligned} \mathbf{u}_k(x, t) &= \int_{\Omega} \mathbf{u}(x, t, \xi) \psi_k(\xi) \tilde{p}(\xi) d\xi = \mathbf{u}_{(L)} \int_{\xi_1}^{\infty} \psi_k(\xi) \tilde{p}(\xi) d\xi \\ &\quad + \int_{\xi_2}^{\xi_1} \mathbf{u}_{(exp)}(x - \xi) \psi_k(\xi) \tilde{p}(\xi) d\xi + \mathbf{u}_{(2)} \int_{\xi_3}^{\xi_2} \psi_k(\xi) \tilde{p}(\xi) d\xi \\ &\quad + \mathbf{u}_{(1)} \int_{\xi_4}^{\xi_3} \psi_k(\xi) \tilde{p}(\xi) d\xi + \mathbf{u}_{(R)} \int_{-\infty}^{\xi_4} \psi_k(\xi) \tilde{p}(\xi) d\xi. \end{aligned} \quad (9.22)$$

The density \tilde{p} and multiwavelet ψ_k are at least piecewise continuous functions, so by (9.22) $\mathbf{u}_k \in C^0$. Now assume that the parametrization ξ of the uncertainty in the location of x_0 has a probability density $\tilde{p} \in C^s(\mathbb{R})$ for some degree of regularity $s \in \mathbb{N}$. There exists a set $\{\psi_i\}_{i=0}^{\infty}$ of polynomials that are orthogonal with respect to \tilde{p} . With this choice of basis functions, we may differentiate (9.22) with respect to x ,

$$\begin{aligned} \frac{\partial}{\partial x} \mathbf{u}_k &= -\mathbf{u}_{(L)} \psi_k(\xi_1) \tilde{p}(\xi_1) + \mathbf{u}_{exp}(x - \xi_1) \psi_k(\xi_1) \tilde{p}(\xi_1) - \mathbf{u}_{exp}(x - \xi_2) \psi_k(\xi_2) \tilde{p}(\xi_2) \\ &\quad + \int_{\xi_2}^{\xi_1} \mathbf{u}'_{(exp)}(x - \xi) \psi_k(\xi) \tilde{p}(\xi) d\xi + \mathbf{u}_{(2)} \psi_k(\xi_2) \tilde{p}(\xi_2) - \mathbf{u}_{(2)} \psi_k(\xi_3) \tilde{p}(\xi_3) \\ &\quad + \mathbf{u}_{(1)} \psi_k(\xi_3) \tilde{p}(\xi_3) - \mathbf{u}_{(1)} \psi_k(\xi_4) \tilde{p}(\xi_4) + \mathbf{u}_{(R)} \psi_k(\xi_4) \tilde{p}(\xi_4), \end{aligned} \quad (9.23)$$

where we used $\partial \xi_i / \partial x = 1$, $i = 1, 2, 3, 4$. In fact, $\mathbf{u}_k(x, t)$ as given by (9.22) is $s + 1$ times differentiable in x or t for $t > 0$ and $\mathbf{u}_k \in C^{s+1}$.

Remark 9.1. Note that the smoothness of \mathbf{u}_k in x and t ultimately depends on the smoothness of \tilde{p} and the choice of basis functions $\{\psi_i\}_{i=0}^{\infty}$, which are all functions of ξ . In contrast, for any fixed value of ξ , the solution $\mathbf{u}(x, t, \xi)$ is discontinuous in the spatial and temporal dimensions, no matter the smoothness of \tilde{p} and $\{\psi_i\}_{i=0}^{\infty}$.

9.2.3 The Stochastic Galerkin Solution Modes

We investigated the smoothness properties of the stochastic modes of the original problems problem (9.5) and (9.2) above, but in all actual computations we solve the modified stochastic Galerkin approximation (9.5)–(9.7). For low-order MW

approximations (small M), the smoothness properties are very different from those derived above. For instance, the $M = 0$ approximation is the deterministic two-phase problem with its characteristic discontinuous solution profile. First-order gPC approximations using a group of orthogonal polynomials and multiwavelets result in linear combinations of deterministic two-phase problems. In terms of regularity, these problems are clearly equivalent to the deterministic problem. Higher-order gPC approximations result in large nonlinear stochastic Galerkin problems that in general cannot be diagonalized into a set of deterministic two-phase problems. Due to their nonlinear nature, we expect these problems to develop discontinuities. However, it is a reasonable assumption that the solution converges to the solution of (9.2). Hence, we assume that the discontinuities get weaker with the order of gPC expansion so that high-order MW approximations have regularity properties that approach the smoothness properties of the analytical stochastic modes.

We have analyzed smoothness of the particular problem of uncertain initial location of the shock in the Riemann problem (9.4). An essential feature of the analysis is that for $t > 0$, the locations of the discontinuities become stochastic. If this were not the case, the gPC coefficients would not be smooth. Thus, for any given set of initial conditions, smoothness should be analyzed in order to determine an appropriate numerical method.

In order to solve (9.5)–(9.7) numerically for arbitrary order M of MW expansion (that may vary in space depending on the smoothness of the solution), we need shock-capturing methods that can account for the discontinuities that are expected due to the stochastic truncation. In regions away from the discontinuities, the solution is at least as smooth as the corresponding deterministic problem, and high-order methods in combination with smooth polynomial stochastic basis functions are more suitable. In the next section, we present a method which combines high-order and shock-capturing methods for the stochastic Galerkin systems.

9.3 Numerical Method

The computational domain is divided into regions of smooth behavior of the solution, and regions of sharp variation. At this stage, these regions are assumed to be known a priori and do not change with time. Thus there is no need to use a detection algorithm to locate the regions of sharp variation apart from flux limiters that are applied for smoothing. However, the methodology may be extended to time-dependent regions (see [7]). A fourth-order Runge-Kutta method is used for the time integration.

9.3.1 Summation-by-Parts Operators

The smooth regions are discretized using a high-order finite difference method based on SBP operators. Boundary conditions are imposed weakly through penalty terms,

where the penalty parameters are chosen such that the numerical method is stable. Operators of order $2n$, $n \in \mathbb{N}$, in the interior of the domain are combined with boundary closures of order of accuracy n .

The first derivative SBP operator was introduced in [13, 22]. Let $\bar{\mathbf{u}}$ denote the uniform spatial discretization of \mathbf{u} . For the first derivative, we use the approximation $\mathbf{u}_x \approx \mathbf{P}^{-1} \mathbf{Q} \bar{\mathbf{u}}$, where subscript x denotes partial derivative and \mathbf{Q} satisfies

$$\mathbf{Q} + \mathbf{Q}^T = \text{diag}(-1, 0, \dots, 0, 1) \equiv \tilde{\mathbf{B}}. \quad (9.24)$$

The property (9.24) is the almost skew-symmetry property introduced in (4.9). For more details about the SBP framework and use of penalty techniques, see Sect. 4.2.2. As held consistently throughout this book, \mathbf{P} must be symmetric and positive definite in order to define a discrete norm. For proof of stability, \mathbf{P} must be diagonal.

9.3.2 HLL Riemann Solver

In the non-smooth regions, MUSCL-type flux limiting [23] is used for reconstruction of the left and right states of the conservative fluxes and advection of the volume fractions. For the conservative problem (9.2), we employ the HLL Riemann solver introduced by Harten et al. [12], defined in (4.27). The fastest signal velocities are given by the maximum and minimum eigenvalues of the Jacobian of the flux. In the deterministic case, the eigenvalues of the Jacobian are known analytically, so the method is inexpensive. For the stochastic Galerkin system, analytical expressions are not available, and numerical approximations of the eigenvalues are used instead. In general, obtaining accurate eigenvalue estimates may be computationally costly. However, for the piecewise constant and piecewise linear multiwavelet expansion, we have explicit expressions for the system eigenvalues due to the constant eigenvectors of the inner triple product matrices A given by (9.10), see Appendix B.2.

The HLL-flux and MUSCL reconstruction are applied to solve the conservative problem (9.7). The (standard) MUSCL scheme is used to solve the advection problem (9.5) in the regions where the solution is expected to be non-smooth. In combination with a suitable Runge-Kutta method, the MUSCL scheme is total variation diminishing (TVD) [9]. For the deterministic solution, this would be a sufficient condition for α to attain physically relevant values only. For the stochastic Galerkin system, we need to ensure that the effect of the artificial dissipation from the flux limiters on the different solution modes does not cause the solution α (linear combination of the modes) to become unphysical. By the TVD property, the expectation mode is restricted to $[0, 1]$, so unphysical values can occur only if the high-order modes are less dissipated than the expectation mode. Artificial dissipation affects highly oscillating functions more than slowly oscillating functions. Since the peaks of the initial functions get sharper with the

order of wavelet chaos, the higher-order modes are increasingly dissipated by the scheme compared to the lower-order modes and the expectation. Thus, most likely the numerical volume fraction always remains restricted to physically relevant values as time is evolved. This evolution is confirmed by the numerical experiments reported later.

9.3.3 Hybrid Scheme

Numerical interfaces can be designed for stable coupling of problems solved separately using SBP operators. The MUSCL scheme can be rewritten in SBP operator form with an artificial dissipation term [1] and can therefore be coupled with other schemes using SBP operators [7]. The coupling requires the artificial dissipation to be zero at the interface in order to enable energy estimates.

The computational domain is divided into a left smooth solution region and a right non-smooth solution region that are weakly coupled with an interface. The leftmost lying part of the right region is a transition region where a second-order one-sided SBP scheme is applied that transitions into the HLL-MUSCL scheme. In this way, there is a stable coupling between the high-order SBP scheme of the left domain and the second-order SBP scheme of the transition region. Numerical dissipation within the order of the scheme is added to the regions where SBP operators are used. Figure 9.2 schematically depicts the hybrid scheme, applied to two spatial grids and coupled with an interface.

9.3.3.1 An Energy Estimate for the Continuous Problem

We will analyze stability for two solution regions coupled by an interface. However, we start with the *continuous* problem on a single domain. In order to do this, we symmetrize the two-phase problem. We assume the existence of a convex entropy function $S(\mathbf{u}^M)$, i.e., the Hessian $\partial^2 S / \partial u_i^M \partial u_j^M$ is positive definite. (Note that convexity as defined here does not allow for zero eigenvalues of the Hessian.) Then, by [11], there exists a variable transformation $\mathbf{w}^M(\mathbf{u}^M) = \partial S / \partial \mathbf{u}^M$ such that $\tilde{\mathbf{f}}(\mathbf{w}^M) = \mathbf{f}(\mathbf{u}^M)$ and

$$\tilde{\mathbf{H}} \mathbf{w}_t^M + \mathbf{J}_w \mathbf{w}_x^M = 0,$$

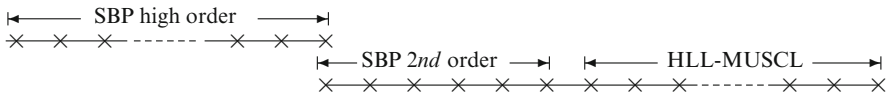


Fig. 9.2 Solution regions on the spatial mesh

where \mathbf{w}^M denotes the vector of MW coefficients of the order M approximation of the transformed variables, and the inverse Hessian $\tilde{\mathbf{H}} = \partial \mathbf{u}^M / \partial \mathbf{w}^M = (\partial^2 S / \partial \mathbf{u}_i^M \partial \mathbf{u}_j^M)^{-1}$ and Jacobian $\mathbf{J}_w = \partial \tilde{\mathbf{f}} / \partial \mathbf{w}$ are symmetric matrices. Due to convexity, $\tilde{\mathbf{H}}$ is positive definite and thus defines a norm. As in the case of the Euler equations, the two-phase equations are homogeneous of degree τ , which implies

$$\tilde{\mathbf{H}} \mathbf{w}^M = \tau \mathbf{u}^M \quad \text{and} \quad \mathbf{J}_w \mathbf{w}^M = \tau \tilde{\mathbf{f}}^M. \quad (9.25)$$

We will use the canonical splittings

$$\mathbf{u}_t^M = \frac{\tau}{1 + \tau} \mathbf{u}_t^M + \frac{1}{1 + \tau} \tilde{\mathbf{H}} \mathbf{w}_t^M, \quad \mathbf{f}_x^M = \frac{\tau}{1 + \tau} \tilde{\mathbf{f}}_x^M + \frac{1}{1 + \tau} \mathbf{J}_w \mathbf{w}_x^M.$$

To obtain an energy estimate for the continuous and stability for the semidiscrete problem, the stochastic Galerkin formulation of the two-phase problem must be homogeneous. To show that this holds under the assumption that the corresponding deterministic problem is homogeneous and some additional assumptions, we consider a deterministic problem that is homogeneous of degree τ . Let

$$\mathbf{J}(\mathbf{u})\mathbf{u} = \tau \mathbf{f}(\mathbf{u}), \quad (9.26)$$

with solution $\mathbf{u} \in \mathbb{R}^n$, Jacobian $\mathbf{J} \in \mathbb{R}^{n \times n}$ and flux $\mathbf{f} \in \mathbb{R}^n$ for a system of n equations. Now assume that the problem satisfying (9.26) is subject to uncertainty in the parameters or in the input conditions. Let J_{ij} denote the (i, j) entry of \mathbf{J} which can be expressed as a truncated MW expansion $J_{ij} = \sum_{k=0}^M (J_{ij})_k \psi_k$. The stochastic Galerkin Jacobian \mathcal{J}^M corresponding to \mathbf{J} consists of $n \times n$ submatrices, each of size $(M+1) \times (M+1)$. Let \mathcal{J}_{ij}^M be the (i, j) submatrix of \mathcal{J}^M , defined by

$$[\mathcal{J}_{ij}^M]_{lm} = \langle \psi_l \psi_m J_{ij} \rangle = \sum_{k=0}^M (J_{ij})_k \langle \psi_k \psi_l \psi_m \rangle, \quad i, j = 1, \dots, n, \quad l, m = 0, \dots, M. \quad (9.27)$$

The stochastic Galerkin flux vector of MW coefficients $\mathbf{f}^M = ((f_1)_0, \dots, (f_1)_M, \dots, (f_n)_0, \dots, (f_n)_M)^T$ is a nonlinear function, and for an arbitrary order M basis of multiwavelets, it is not uniquely defined. To see this, with the pseudospectral product $*$ defined in (9.9), in general

$$(a * b) * c \neq a * (b * c)$$

for MW approximations of stochastic functions $a(\xi)$, $b(\xi)$, $c(\xi)$, each one truncated to some order M . This implies that the definition of the stochastic Galerkin flux \mathbf{f}^M depends on the order in which pseudospectral operations are performed when evaluating \mathbf{f}^M . Hence, it is not uniquely defined. We may now either restrict

ourselves to MW bases where the order of pseudospectral operations does not matter e.g., Haar wavelets, or we may restrict the order in which pseudospectral operations are performed so as to make sure that mathematical properties of interest, such as, homogeneity, are satisfied. We take the latter approach and define the order M approximation of \mathbf{f} through its MW coefficients by

$$(f_i)_k \equiv \frac{1}{\tau} \sum_{j=1}^n (J_{ij} * u_j)_k, \quad i = 1, \dots, n, \quad k = 0, \dots, M, \quad (9.28)$$

which is consistent with the deterministic homogeneous problem. Note that relation (9.28) is essentially just a restriction on the order of pseudospectral operations in the calculation of \mathbf{f} . It stipulates that \mathbf{f} must be defined in terms of the approximation of \mathbf{J} . Clearly, the approximation of \mathbf{J} should also be as close to the true (i.e., infinite order MW expansion) \mathbf{J} as possible. However, for the energy estimates that require homogeneity of the stochastic Galerkin formulation, we only need to satisfy (9.28).

Proposition 9.1. *Assume that the deterministic problem (9.26) holds, and for a consistent pseudospectral approximation \mathcal{J}^M of \mathbf{J} , let the stochastic Galerkin flux \mathbf{f}^M be given by the MW coefficients as defined in (9.28). Then the stochastic Galerkin formulation of order M is also homogeneous of degree τ , i.e., it satisfies*

$$\mathcal{J}^M(\mathbf{u}^M)\mathbf{u}^M = \tau \mathbf{f}^M(\mathbf{u}^M), \quad (9.29)$$

where $\mathbf{u}^M = ((u_1)_0, \dots, (u_1)_M, \dots, (u_n)_0, \dots, (u_n)_M)^T \in \mathbb{R}^{n(M+1)}$ and $\mathbf{f}^M = ((f_1)_0, \dots, (f_1)_M, \dots, (f_n)_0, \dots, (f_n)_M)^T \in \mathbb{R}^{n(M+1)}$.

Proof. Using the notation (9.10) for the pseudospectral product $*$, by (9.27) the (i, j) submatrix of \mathcal{J}^M can be written

$$\mathcal{J}_{ij}^M = \mathbf{A}(\mathbf{J}_{ij}^M), \quad i, j = 1, \dots, n,$$

where $\mathbf{J}_{ij}^M = ((J_{ij})_0, \dots, (J_{ij})_M)^T$. Thus, we have

$$\mathcal{J}^M = \begin{bmatrix} \mathbf{A}(\mathbf{J}_{11}^M) & \dots & \mathbf{A}(\mathbf{J}_{1n}^M) \\ \vdots & \ddots & \vdots \\ \mathbf{A}(\mathbf{J}_{n1}^M) & \dots & \mathbf{A}(\mathbf{J}_{nn}^M) \end{bmatrix}.$$

By the relation (9.28), any subvector $\mathbf{f}_i^M = ((f_i)_0, \dots, (f_i)_M)^T$ of the total flux vector of MW coefficients \mathbf{f}^M can be written

$$\mathbf{f}_i^M = \frac{1}{\tau} \sum_{j=1}^n \mathbf{A}(\mathbf{J}_{ij}^M)\mathbf{u}_j^M, \quad i = 1, \dots, n.$$

Then, considering the i th row of submatrices, we have

$$[\mathcal{J}^M \mathbf{u}^M]_i = \sum_{j=1}^n \mathcal{J}_{ij}^M \mathbf{u}_j^M = \sum_{j=1}^n \mathbf{A}(\mathbf{J}_{ij}^M) \mathbf{u}_j^M = \tau \mathbf{f}_i^M, \quad i = 1, \dots, n,$$

which is equal to (9.29).

Remark 9.2. The original (deterministic) Jacobian entries J_{ij} are nonlinear functions of u , and the stochastic Galerkin counterpart \mathcal{J}^M is a nonlinear function of the gPC coefficients of u . Since the approximation of a nonlinear stochastic function by means of pseudospectral operations depends on the order in which the operations are performed, the matrix \mathcal{J}^M is not uniquely defined unless we specify the order. However, for proof of Proposition 9.1, it is sufficient to define \mathbf{f}^M as a function of \mathcal{J}^M , but there is no need to specify \mathcal{J}^M in terms of the order of pseudospectral operations.

We will now derive an energy estimate for the continuous symmetrized formulation of the stochastic Galerkin Euler equations in split form,

$$\frac{\tau}{1+\tau} \mathbf{u}_t^M + \frac{1}{1+\tau} \tilde{\mathbf{H}} \mathbf{w}_t^M + \frac{\tau}{1+\tau} \tilde{\mathbf{f}}_x^M + \frac{1}{1+\tau} \mathbf{J}_w \mathbf{w}_x = 0. \quad (9.30)$$

Under the conditions of Proposition 9.1, multiply (9.30) by $(1+\tau)(\mathbf{w}^M)^T$ and integrate over the physical domain. We get

$$\begin{aligned} & \tau \int_0^1 (\mathbf{w}^M)^T \mathbf{u}_t^M dx + \int_0^1 (\mathbf{w}^M)^T \tilde{\mathbf{H}} \mathbf{w}_t^M dx + \tau \int_0^1 (\mathbf{w}^M)^T \tilde{\mathbf{f}}_x^M dx \\ & + \int_0^1 (\mathbf{w}^M)^T \mathbf{J}_w \mathbf{w}_x^M dx = \int_0^1 \left((\mathbf{w}^M)^T (\tilde{\mathbf{H}} \mathbf{w}^M)_t + (\mathbf{w}^M)^T \tilde{\mathbf{H}} \mathbf{w}_t^M \right) dx \\ & + \int_0^1 \left((\mathbf{w}^M)^T (\mathbf{J}_w \mathbf{w}^M)_x + (\mathbf{w}^M)^T \mathbf{J}_w \mathbf{w}_x^M \right) dx \\ & = \frac{d}{dt} \|\mathbf{w}^M\|_{\tilde{\mathbf{H}}} + [(\mathbf{w}^M)^T \mathbf{J}_w \mathbf{w}^M]_0^1 = 0, \end{aligned} \quad (9.31)$$

where the first equality follows from (9.25). The generalized energy estimate (9.31) is a straightforward stochastic Galerkin generalization of that given for the deterministic problem in [8].

9.3.3.2 Stability in a Single Domain

Next we consider the *semidiscrete* problem and start with a single domain. The stability analysis is a direct generalization of the stability of the symmetrized Euler

equations in [8]. We define the flux and the Jacobian under the conditions of Proposition 9.1 which implies that the stochastic Galerkin system is homogeneous. Let \vec{u}^M and \vec{w}^M denote the spatial discretizations of u^M and w^M , respectively, on a mesh consisting of m equidistant gridpoints. Let $E_1 = \text{diag}(1, 0, \dots, 0)$ and $E_m = \text{diag}(0, \dots, 0, 1)$. The semidiscretized scheme is

$$\begin{aligned} & \frac{\tau}{1+\tau} \vec{u}_t^M + \frac{1}{1+\tau} \hat{H} \vec{w}_t^M + \frac{\tau}{1+\tau} (\mathbf{P}^{-1} \mathbf{Q} \otimes \mathbf{I}) \tilde{f}^M(\vec{w}^M) \\ & + \frac{1}{1+\tau} \hat{J}_w(\mathbf{P}^{-1} \mathbf{Q} \otimes \mathbf{I}) \vec{w}^M \\ & = (\mathbf{P}^{-1} E_1 \otimes \Sigma_1^w)(\vec{w}^M - \vec{g}_1) + (\mathbf{P}^{-1} E_m \otimes \Sigma_m^w)(\vec{w}^M - \vec{g}_m), \end{aligned} \quad (9.32)$$

where \hat{H} is block diagonal with each diagonal block equal to \tilde{H} evaluated at the spatial points. Σ_1^w and Σ_m^w are penalty matrices to be determined, and \vec{g}_1 and \vec{g}_m are vectors where only the entries corresponding to the left and right boundaries are allowed nonzero values. We assume a diagonal norm \mathbf{P} , so $(\mathbf{P} \otimes \mathbf{I}) \hat{H} = \hat{H} (\mathbf{P} \otimes \mathbf{I})$. Also, \hat{J}_w commutes with $(\mathbf{P} \otimes \mathbf{I})$. In order to show stability, we may assume homogeneous boundary conditions $\vec{g}_1 = \vec{g}_m = 0$. Multiplying (9.32) from the left by $(1 + \tau)(\vec{w}^M)^T (\mathbf{P} \otimes \mathbf{I})$ and using the homogeneity properties of (9.25) yields

$$\begin{aligned} & \frac{d}{dt} \|\vec{w}^M\|_{(\mathbf{P} \otimes \mathbf{I}) \hat{H}}^2 + (\vec{w}^M)^T \left((\mathbf{Q} \otimes \mathbf{I}) \hat{J}_w + \hat{J}_w (\mathbf{Q} \otimes \mathbf{I}) \right) \vec{w}^M \\ & = (1 + \tau) (\vec{w}^M)_1^T \Sigma_1^w \vec{w}_1^M + (1 + \tau) \vec{w}_m^T \Sigma_m^w \vec{w}_m^M. \end{aligned} \quad (9.33)$$

Add the transpose of (9.33) to itself and use the SBP relation (9.24)

$$\begin{aligned} \frac{d}{dt} \|\vec{w}^M\|_{(\mathbf{P} \otimes \mathbf{I}) \hat{H}}^2 & = \vec{w}_1^T \left(\mathbf{J}_w(\vec{w}_1^M) + (1 + \tau) \Sigma_1^w \right) \vec{w}_1^M \\ & \quad + (\vec{w}_m^M)^T \left(-\mathbf{J}_w(\vec{w}_m^M) + (1 + \tau) \Sigma_m^w \right) \vec{w}_m^M. \end{aligned} \quad (9.34)$$

The scheme is stable in the sense of Definition 1.3 with the penalties

$$\Sigma_1^w = -\delta_1 \mathbf{J}_w^+(\vec{w}_1^M), \quad \Sigma_m^w = \delta_m \mathbf{J}_w^-(\vec{w}_m^M), \quad \delta_1, \delta_m \geq \frac{1}{1 + \tau}.$$

Remark 9.3. The stability analysis above follows that in [8]; for the case $M = 0$ the analysis is in fact identical. We show here that the analysis in [8] generalizes to the stochastic Galerkin formulation of order M of multiwavelet expansion under the conditions of Proposition 9.1.

9.3.3.3 Stability at the Interface

Now consider a problem with two domains connected by an interface. A grid point at the interface will be assigned two solution values, one from each of the stencils that meet at the interface. The difference between the solutions at the interface are penalized analogously to the treatment of the (outer) boundary conditions we have seen in the single domain stability analysis. By ignoring the imposition of boundary conditions, the semidiscrete systems of the left and right domains are given by

$$\begin{aligned} \frac{\tau}{1+\tau}(\bar{\mathbf{u}}_L^M)_t + \frac{1}{1+\tau}\hat{\mathbf{H}}(\bar{\mathbf{w}}_L^M)_t + \frac{\tau}{1+\tau}(\mathbf{P}_L^{-1}\mathbf{Q}_L \otimes \mathbf{I})\tilde{\mathbf{f}}^M(\bar{\mathbf{w}}_L^M) \\ + \frac{1}{1+\tau}\tilde{\mathbf{J}}_w(\mathbf{P}_L^{-1}\mathbf{Q}_L \otimes \mathbf{I})\bar{\mathbf{w}}_L^M = (\mathbf{P}_L^{-1}\mathbf{E}_m \otimes \boldsymbol{\Sigma}_L^w)(\bar{\mathbf{w}}_{m,L}^M - \bar{\mathbf{w}}_{1,R}^M), \end{aligned} \quad (9.35)$$

and

$$\begin{aligned} \frac{\tau}{1+\tau}(\bar{\mathbf{u}}_R^M)_t + \frac{1}{1+\tau}\tilde{\mathbf{J}}_u(\bar{\mathbf{w}}_R^M)_t + \frac{\tau}{1+\tau}(\mathbf{P}_R^{-1}\mathbf{Q}_R \otimes \mathbf{I})\tilde{\mathbf{f}}^M(\bar{\mathbf{w}}_R^M) \\ + \frac{1}{1+\tau}\tilde{\mathbf{J}}_w(\mathbf{P}_R^{-1}\mathbf{Q}_R \otimes \mathbf{I})\bar{\mathbf{w}}_R^M = (\mathbf{P}_R^{-1}\mathbf{E}_1 \otimes \boldsymbol{\Sigma}_R^w)(\bar{\mathbf{w}}_{1,R}^M - \bar{\mathbf{w}}_{m,L}^M), \end{aligned} \quad (9.36)$$

respectively. We follow the procedure of Sect. 9.3.3.2. Multiplying (9.35) from the left by $(1+\tau)(\bar{\mathbf{w}}_L^M)^T(\mathbf{P}_L \otimes \mathbf{I})$ and using the homogeneity identity (9.25), we have

$$\begin{aligned} \frac{d}{dt} \left\| \bar{\mathbf{w}}_L^M \right\|_{(\mathbf{P}_L \otimes \mathbf{I})\hat{\mathbf{H}}}^2 + (\bar{\mathbf{w}}_L^M)^T(\mathbf{Q}_L \otimes \mathbf{I})\tilde{\mathbf{J}}_w\bar{\mathbf{w}}_L^M + (\bar{\mathbf{w}}_L^M)^T\tilde{\mathbf{J}}_w(\mathbf{Q}_L \otimes \mathbf{I})\bar{\mathbf{w}}_L^M \\ = (1+\tau)\bar{\mathbf{w}}_{m,L}^M\boldsymbol{\Sigma}_L^w(\bar{\mathbf{w}}_{m,L}^M - \bar{\mathbf{w}}_{1,R}^M). \end{aligned} \quad (9.37)$$

Adding the transpose of (9.37) to itself, neglecting the outer boundaries and performing similar operations on (9.36), we get

$$\begin{aligned} \frac{d}{dt} \left(\left\| \bar{\mathbf{w}}_L^M \right\|_{(\mathbf{P}_L \otimes \mathbf{I})\hat{\mathbf{H}}}^2 + \left\| \bar{\mathbf{w}}_R^M \right\|_{(\mathbf{P}_R \otimes \mathbf{I})\hat{\mathbf{H}}}^2 \right) + (\bar{\mathbf{w}}_{m,L}^M)^T\mathbf{J}_w(\bar{\mathbf{w}}_{m,L}^M)\bar{\mathbf{w}}_{m,L}^M \\ - (\bar{\mathbf{w}}_{1,R}^M)^T\mathbf{J}_w(\bar{\mathbf{w}}_{1,R}^M)\bar{\mathbf{w}}_{1,R}^M = (1+\tau)(\bar{\mathbf{w}}_{m,L}^M)^T\boldsymbol{\Sigma}_L^w(\bar{\mathbf{w}}_{m,L}^M - \bar{\mathbf{w}}_{1,R}^M) \\ + (1+\tau)(\bar{\mathbf{w}}_{1,R}^M)^T\boldsymbol{\Sigma}_R^w(\bar{\mathbf{w}}_{1,R}^M - \bar{\mathbf{w}}_{m,L}^M). \end{aligned} \quad (9.38)$$

Assuming symmetric $\boldsymbol{\Sigma}_L^w$ and $\boldsymbol{\Sigma}_R^w$, we get the stability condition

$$\begin{bmatrix} \bar{\mathbf{w}}_{m,L}^M \\ \bar{\mathbf{w}}_{1,R}^M \end{bmatrix}^T \begin{bmatrix} -\mathbf{J}_w(\bar{\mathbf{w}}_{m,L}^M) + (1+\tau)\boldsymbol{\Sigma}_L^w & -\frac{1+\tau}{2}(\boldsymbol{\Sigma}_L^w + \boldsymbol{\Sigma}_R^w) \\ -\frac{1+\tau}{2}(\boldsymbol{\Sigma}_L^w + \boldsymbol{\Sigma}_R^w) & \mathbf{J}_w(\bar{\mathbf{w}}_{1,R}^M) + (1+\tau)\boldsymbol{\Sigma}_R^w \end{bmatrix} \begin{bmatrix} \bar{\mathbf{w}}_{m,L}^M \\ \bar{\mathbf{w}}_{1,R}^M \end{bmatrix} \leq 0. \quad (9.39)$$

Being in the smooth domain, we assume $\mathbf{J}_w(\vec{w}_{m,L}^M) = \mathbf{J}_w(\vec{w}_{1,R}^M) = \mathbf{J}$ and obtain stability with

$$\Sigma_L^w = \frac{1}{1+\tau} \mathbf{J} - \boldsymbol{\theta}, \quad \Sigma_R^w = -\frac{1}{1+\tau} \mathbf{J} - \boldsymbol{\theta},$$

where $\boldsymbol{\theta}$ is a positive semidefinite matrix. This is completely analogous to the penalties derived in the constant advection problem presented in [7].

The penalties derived in the stability analysis apply to the entropy variables w , but in the numerical experiments we use a conservative formulation for correct shock speed and employ the conservative variables u . Therefore we need to transform the penalties to the conservative variables. Assuming that the solution is smooth and $\tilde{\mathbf{H}}(\vec{w}_{m,L}^M) = \tilde{\mathbf{H}}(\vec{w}_{1,R}^M)$, we rewrite the interface terms

$$\begin{aligned} \Sigma_L^w(\vec{w}_{m,L}^M - \vec{w}_{1,R}^M) &= \frac{1}{1+\tau} \mathbf{J}(\vec{w}_{m,L}^M - \vec{w}_{1,R}^M) - \boldsymbol{\theta}(\vec{w}_{m,L}^M - \vec{w}_{1,R}^M) \\ &= \frac{1}{1+\tau} \left(\tilde{f}^M(\vec{w}_{m,L}^M) - \tilde{f}^M(\vec{w}_{1,R}^M) \right) \\ &\quad - \boldsymbol{\theta} \tau \left(\tilde{\mathbf{H}}^{-1}(\vec{w}_{m,L}^M) \vec{u}_{m,L}^M - \tilde{\mathbf{H}}^{-1}(\vec{w}_{1,R}^M) \vec{u}_{1,R}^M \right) \\ &= \frac{1}{1+\tau} \left(f^M(\vec{u}_{m,L}^M) - f^M(\vec{u}_{1,R}^M) \right) - \hat{\boldsymbol{\theta}} \left(\vec{u}_{m,L}^M - \vec{u}_{1,R}^M \right) \\ &= \left(\frac{1}{1+\tau} \mathbf{J}_u - \hat{\boldsymbol{\theta}} \right) \left(\vec{u}_{m,L}^M - \vec{u}_{1,R}^M \right) = \Sigma_L^u \left(\vec{u}_{m,L}^M - \vec{u}_{1,R}^M \right), \end{aligned} \quad (9.40)$$

where

$$\mathbf{J}_u = \left. \frac{\partial f^M}{\partial \mathbf{u}^M} \right|_{x=x_{int}},$$

and

$$\Sigma_L^u = \frac{1}{1+\tau} \mathbf{J}_u - \hat{\boldsymbol{\theta}}, \quad (9.41)$$

and $\hat{\boldsymbol{\theta}} = \tau \boldsymbol{\theta} \tilde{\mathbf{H}}^{-1}$ is a positive semidefinite matrix for $\tau > 0$ since $\tilde{\mathbf{H}}$ is positive definite and $\boldsymbol{\theta}$ is positive semidefinite. Similarly, we get the right penalty matrix

$$\Sigma_R^u = -\frac{1}{1+\tau} \mathbf{J}_u - \hat{\boldsymbol{\theta}}. \quad (9.42)$$

With the penalty matrices (9.41) and (9.42), we obtain stability, as defined in Definition 1.3.

9.3.3.4 Conservation at the Interface

In order to show conservation over the interface, we mimic the continuous case where we multiply the conservative formulation by a smooth function ϕ , integrate by parts to get

$$\int_0^{x_{int}} \phi u_t dx + \int_{x_{int}}^1 \phi u_t dx = \int_0^{x_{int}} \phi_x f(u) dx + \int_{x_{int}}^1 \phi_x f(u) dx + B.T., \quad (9.43)$$

where $B.T.$ denotes outer boundary terms. In (9.43) no interface terms are present. Consider the semidiscrete scheme

$$(\vec{u}_L^M)_t + (\mathbf{P}_L^{-1} \mathbf{Q}_L \otimes \mathbf{I}) \mathbf{f}^M(\vec{u}_L^M) = (\mathbf{P}_L^{-1} \mathbf{E}_m \otimes \boldsymbol{\Sigma}_L^u) (\vec{u}_{m,L}^M - \vec{u}_{1,R}^M) \quad (9.44)$$

$$(\vec{u}_R^M)_t + (\mathbf{P}_R^{-1} \mathbf{Q}_R \otimes \mathbf{I}) \mathbf{f}^M(\vec{u}_R^M) = (\mathbf{P}_R^{-1} \mathbf{E}_1 \otimes \boldsymbol{\Sigma}_R^u) (\vec{u}_{1,R}^M - \vec{u}_{m,L}^M). \quad (9.45)$$

Multiplying from the left by $\vec{\phi}_L^T (\mathbf{P}_L \otimes \mathbf{I})$ and $\vec{\phi}_R^T (\mathbf{P}_R \otimes \mathbf{I})$, respectively, where $\vec{\phi}_L$ and $\vec{\phi}_R$ are discretized smooth functions satisfying $\vec{\phi}_{m,L} = \vec{\phi}_{1,R} = \vec{\phi}_I$, we get

$$\begin{aligned} \vec{\phi}_L^T (\mathbf{P}_L \otimes \mathbf{I}) (\vec{u}_L^M)_t + \vec{\phi}_R^T (\mathbf{P}_R \otimes \mathbf{I}) (\vec{u}_R^M)_t &= (\mathbf{D}_L \vec{\phi}_L)^T (\mathbf{P}_L \otimes \mathbf{I}) \mathbf{f}^M(\vec{u}_L^M) \\ &\quad + (\mathbf{D}_R \vec{\phi}_R)^T (\mathbf{P}_R \otimes \mathbf{I}) \mathbf{f}^M(\vec{u}_R^M) + B.T. \\ + \vec{\phi}_I^T [(\vec{u}_{m,L}^M - \vec{u}_{1,R}^M) (\boldsymbol{\Sigma}_L^u - \boldsymbol{\Sigma}_R^u) - \mathbf{f}^M(\vec{u}_{m,L}^M) + \mathbf{f}^M(\vec{u}_{1,R}^M)] &= 0. \end{aligned} \quad (9.46)$$

The semidiscrete formulation (9.46) mimics the continuous expression (9.43) if we choose $\boldsymbol{\Sigma}_L^u$ and $\boldsymbol{\Sigma}_R^u$ such that

$$(\vec{u}_{m,L}^M - \vec{u}_{1,R}^M) (\boldsymbol{\Sigma}_L^u - \boldsymbol{\Sigma}_R^u) - \mathbf{f}^M(\vec{u}_{m,L}^M) + \mathbf{f}^M(\vec{u}_{1,R}^M) = \mathbf{0}.$$

We assume $\mathbf{J}_w(\vec{w}_{m,L}^M) = \mathbf{J}_w(\vec{w}_{1,R}^M) = \mathbf{J}$. Then, the interface terms cancel with the choice $\boldsymbol{\Sigma}_L^u - \boldsymbol{\Sigma}_R^u = \mathbf{J}$, which is consistent with the condition for stability given by the penalties (9.41) and (9.42) and $\tau = 1$.

9.4 Numerical Results

The exact solution of the test problem is known analytically for any given value of the stochastic variable ξ . Thus, we can obtain the exact statistics to arbitrary accuracy by averaging the exact Riemann solutions over a large number of realizations

of ξ . In the numerical experiments, we will assume $\xi \sim \mathcal{U}[-0.05, 0.05]$, where \mathcal{U} denotes the uniform distribution. For the numerical solutions, we use SBP operators that can be found in [15].

9.4.1 Convergence of Smooth Solutions

The method of manufactured solutions is used to impose a smooth timedependent solution of the two-phase problem through a source term. We consider the manufactured solution defined by

$$\begin{aligned}\alpha &= \alpha_0 + \alpha_1 \tanh(s(x_0 - x + t + \xi)) \\ \beta &= \beta_0 + \beta_1 \tanh(-s(x_0 - x + t + \xi)) \\ v &= \tanh(s(v_0 + x_0 - x + t + \xi)) + \tanh(-s(-v_0 + x_0 - x + t + \xi)) \\ p &= p_0 + p_1 \tanh(s(x_0 - x + t + \xi)),\end{aligned}$$

with $s = 15$, $v_0 = 0.03$, $\alpha_0 = \alpha_1 = \beta_0 = \beta_1 = 0.5$, $p_0 = 0.75$, $p_1 = 0.25$. We take $\rho_\alpha = 1$ and $\rho_\beta = 0.125$. We measure the error in the $L_2(\Omega, \mathcal{P})$ norm and the discrete ℓ_2 norm,

$$\begin{aligned}\|\bar{\mathbf{u}}^M - \bar{\mathbf{u}}\|_{2,2} &\equiv \|\bar{\mathbf{u}}^M - \bar{\mathbf{u}}\|_{\ell_2, L_2(\Omega, \mathcal{P})} \\ &= \left(\Delta x \sum_{i=1}^m \left\| \bar{\mathbf{u}}^M(x_i, t, \xi) - \bar{\mathbf{u}}(x_i, t, \xi) \right\|_{L_2(\Omega, \mathcal{P})}^2 \right)^{1/2} \\ &= \left(\Delta x \sum_{i=1}^m \int_{\Omega} (\bar{\mathbf{u}}^M(x_i, t, \xi) - \bar{\mathbf{u}}(x_i, t, \xi))^2 d\mathcal{P}(\xi) \right)^{1/2} \\ &\approx \left(\Delta x \sum_{i=1}^m \sum_{j=1}^q (\bar{\mathbf{u}}^M(x_i, t, \xi_q^{(j)}) - \bar{\mathbf{u}}(x_i, t, \xi_q^{(j)}))^2 w_q^{(j)} \right)^{1/2},\end{aligned}\tag{9.47}$$

where a q -point quadrature rule with points $\{\xi_q^{(j)}\}_{j=1}^q$ and weights $\{w_q^{(j)}\}_{j=1}^q$ was used in the last line to approximate the integral in ξ . The Gauss-Legendre quadrature is used here since the solution is smooth in the stochastic dimension.

Figure 9.3a shows the spatial convergence when the proportion of low-order and high-order points remains constant. The low-order scheme dominates the error, so the overall convergence rate is second-order. In regions of fourth-order operators, the error levels are lower and therefore the local accuracy higher compared to the regions of second-order operators, see Fig. 9.3b. This is further illustrated in

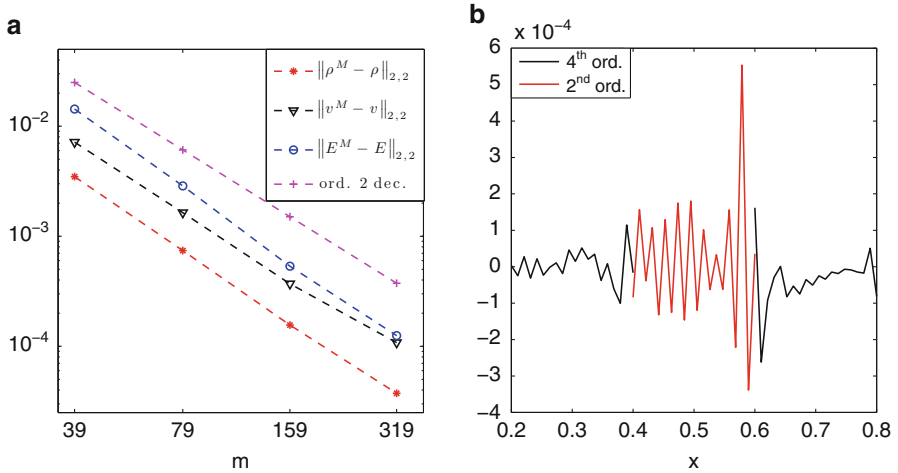


Fig. 9.3 SBP 4-2-4, fixed proportion of SBP 2 points. $N_p = 8$, $N_r = 0$ order of multiwavelets (Legendre polynomials). (a) 2,2 norm of errors for smooth solution, $t = 0.05$. (b) Error in mean density, $t = 0.1$

Fig. 9.4 Comparison of 2,2 norm of errors, three solution regions SBP 2-4-2 versus a single region solved with SBP 2, $t = 0.1$. The proportion of fourth-order points remains constant during mesh refinement. $N_p = 8$, $N_r = 0$ order of multiwavelets (Legendre polynomials)

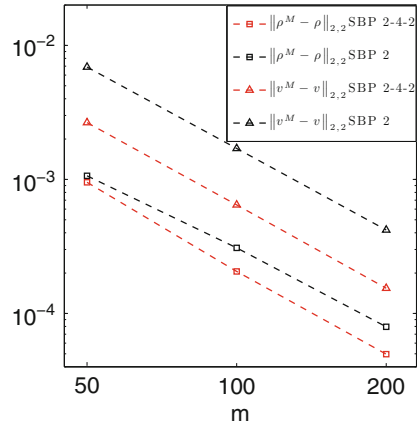


Fig. 9.4, where a similar problem with sharp gradients in the middle of the domain is solved with a hybrid scheme where fourth-order operators are used for the region of large gradients and second-order operators are used for the regions next to the boundaries. With a constant proportion of high-order points under mesh refinement, the convergence is second-order. Comparison with the solution with second-order operators throughout the computational domain, also included in Fig. 9.4, shows that the error of the hybrid scheme is smaller.

Figure 9.5a shows the spatial convergence employing three computational domains separated by two interfaces. The middle domain is solved with second-order SBP and the left and right domains with fourth-order SBP. The number of points in the second-order region remains constant (20), as the high-order domains

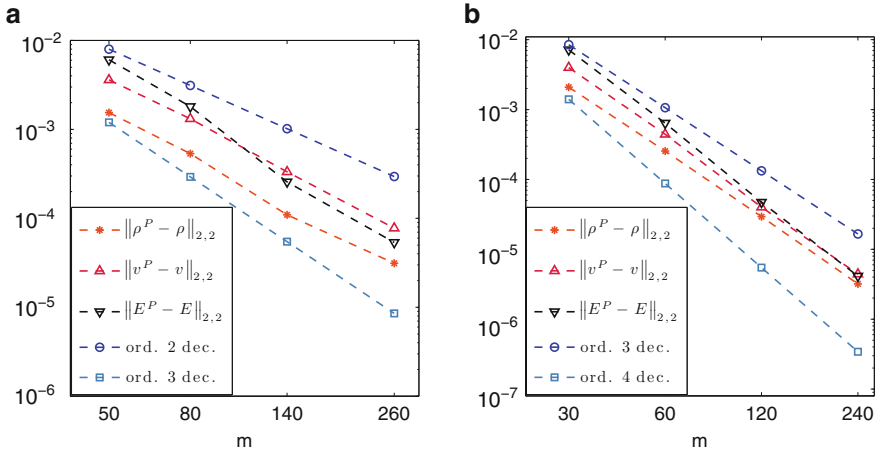


Fig. 9.5 Spatial convergence with three regions and two interfaces. $t = 0.05$, $N_p = 8$, $N_r = 0$ order of multiwavelets (Legendre polynomials). Superscript P denotes the numerical gPC solution. (a) SBP4-SBP2-SBP4, fixed number of SBP2 points. (b) Three SBP4 schemes coupled by two interfaces

are refined. Figure 9.5b depicts the spatial convergence with three domains, all solved with fourth-order SBP. The proportion of points in each region remains the same, so the interface locations do not change when the grids are refined.

9.4.2 Non-smooth Riemann Problem

With the hybrid scheme as depicted schematically in Fig. 9.2, we solve the problems (9.5)–(9.7) with the boundary conditions in (9.4) and assuming $\xi \sim \mathcal{U}[-0.05, 0.05]$. Figure 9.6 shows the variances of density, velocity, energy, and pressure at $t = 0.05$. The error from the interface is not significant compared to the error due to the stochastic truncation and spatial resolution. A relatively fine mesh and high-order MW expansion is required to capture the variance of the solution. Especially high-order MW coefficients exhibit sharp spatial variation. Thus, to attain a given level of accuracy, more spatial gridpoints are required for the stochastic Galerkin problem compared to the deterministic problem.

Figure 9.7 depicts the convergence of pressure statistics with increasing order of MW on a fixed spatial grid of 400 points. In the analysis of regularity in Sect. 9.2, we anticipated the solution to develop a larger number of weaker discontinuities as the order of MW expansion increases. This behavior can be observed in Fig. 9.7. All (visible) discontinuities are located in the right domain where the shock-capturing method is used.

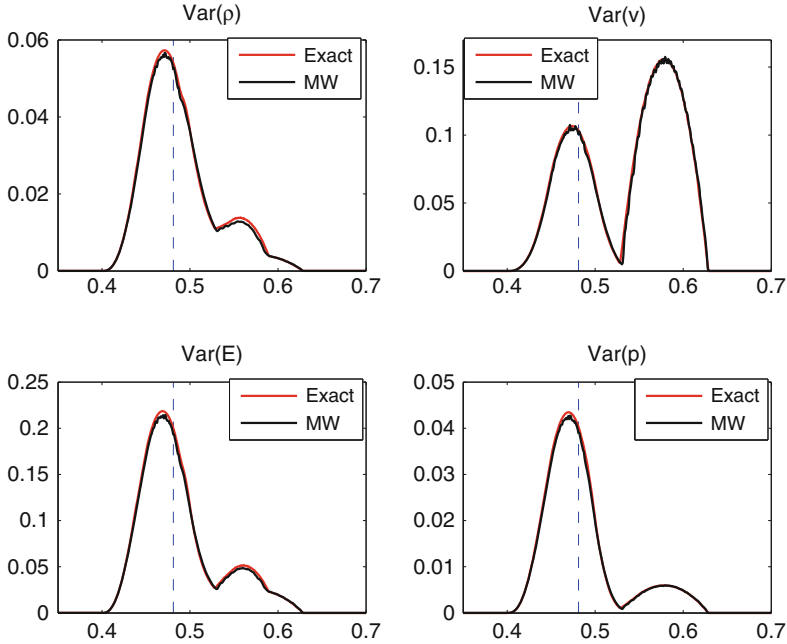


Fig. 9.6 Variances at $t = 0.05$, $m = 400$, fourth order SBP (left region) single interface (dashed blue line) and HLL-MUSCL (right region), $(N_p, N_r) = (0, 5)$ (Haar wavelets)

9.5 Summary and Conclusions

In order to efficiently solve fluid flow problems, a feasible strategy is to locally adapt the numerical method to the smoothness of the solution whenever these properties are known or can be estimated. Stochastic Galerkin formulation of a stochastic hyperbolic problem typically leads to a problem that develops multiple discontinuities in finite time. If these discontinuities are all contained within a known spatial region in a time interval of interest, a shock-capturing method should be used for the corresponding grid points. For the regions of smooth solution, high-order methods should be used. The different methods must be coupled to maintain stability and propagate information accurately over the interfaces between the domains. Note that the solution is unknown in the interior, so one cannot treat the interfaces like boundaries with known boundary conditions. A two-phase Riemann problem with uncertain initial discontinuity location has been investigated with respect to the smoothness properties of the MW coefficients of the solution. Whereas the corresponding deterministic problem has a discontinuous solution profile, the stochastic modes of the gPC expansion of the true solution are smooth.

A symmetrization and combination of conservative and non-conservative formulation leads to a generalized energy estimate for the stochastic Galerkin system, just as for the case of the deterministic Euler equations. Under certain smoothness

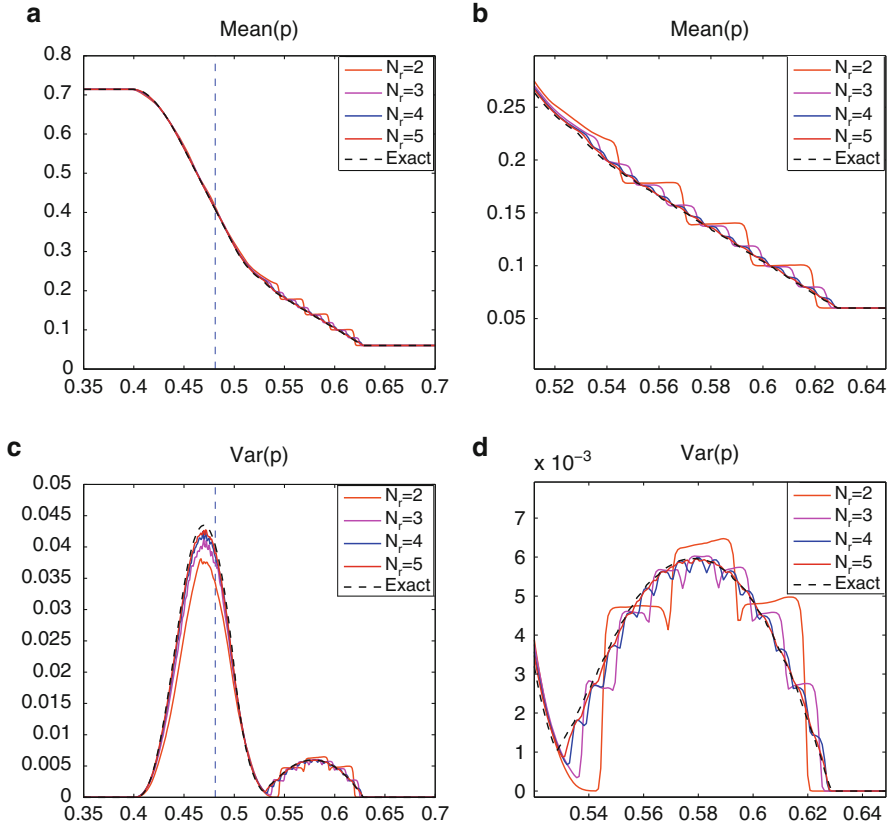


Fig. 9.7 Convergence of the mean and variance of pressure with the order of MW chaos, different orders of piecewise constant MW. $t = 0.05$, $m = 400$. Fourth-order SBP (left domain) and HLL-MUSCL (right domain). (a) Mean pressure. (b) Mean pressure in the proximity of the deterministic shock. (c) Variance of pressure. (d) Variance of pressure in the proximity of the deterministic shock

assumptions, stability at the interfaces can be obtained for the symmetrized system. The derived penalty matrices are transformed back to the conservative variable formulation that is used in the numerical experiments.

The numerical results show that the convergence rate for the smooth problem (smoothness enforced by the method of manufactured solutions) is second-order when fourth-order and second-order operators are combined and the proportion of second-order points remains constant during mesh refinement. However, the error is smaller in this case compared to the case of a single domain solved with second-order operators.

The two-phase non-smooth Riemann problem is reasonably well resolved with the hybrid scheme combining high-order SBP operators in the smooth regions with the HLL solver and MUSCL reconstruction in the spatial region containing

discontinuities. A relatively large number of multiwavelets is needed to accurately represent the stochastic solution. This in turn requires a fine spatial mesh for accurate resolution.

The framework presented here can be extended to time-dependent interfaces that are adapted to the evolving regions of non-smooth solutions. A moving mesh based on interfaces and SBP-operators has already been designed for deterministic problems in [7], and this technique could be used for stochastic Galerkin systems. Depending on the problem, different MW bases can be used in the different spatial regions for efficient representation of the local uncertainty. Alternative techniques include adaptive stochastic bases that evolve in space and time for optimal representation of localized phenomena.

In the case of a moving interface, several detection strategies can be used relying either on the physical solution, e.g., $\alpha = 0.5$, or on the overall variance which would provide a measure of the oscillations. Further investigations are required to identify the most effective detection algorithm.

References

1. Abbas Q, van der Weide E, Nordström J (2009) Accurate and stable calculations involving shocks using a new hybrid scheme. In: Proceedings of the 19th AIAA CFD conference, no. 2009-3985. Conference Proceeding Series. AIAA, San Antonio, TX.
2. Carpenter MH, Nordström J, Gottlieb D (1999) A stable and conservative interface treatment of arbitrary spatial accuracy. *J Comput Phys* 148(2):341–365. doi:<http://dx.doi.org/10.1006/jcph.1998.6114>
3. Chen M, Keller AA, Lu Z, Zhang D, Zyvoloski G (2008) Uncertainty quantification for multiphase flow in random porous media using KL-based moment equation approaches. In: AGU spring meeting abstracts, p A2, Fort Lauderdale, FL.
4. Chen QY, Gottlieb D, Hesthaven JS (2005) Uncertainty analysis for the steady-state flows in a dual throat nozzle. *J Comput Phys* 204(1):378–398. doi:<http://dx.doi.org/10.1016/j.jcp.2004.10.019>
5. Deb MK, Babuška IM, Oden JT (2001) Solution of stochastic partial differential equations using Galerkin finite element techniques. *Comput Methods Appl Math* 190(48):6359–6372. doi:[10.1016/S0045-7825\(01\)00237-7](https://doi.org/10.1016/S0045-7825(01)00237-7), <http://www.sciencedirect.com/science/article/pii/S0045782501002377>
6. Debusschere BJ, Najm HN, Pébay PP, Knio OM, Ghanem RG, Le Maître OP (2005) Numerical challenges in the use of polynomial chaos representations for stochastic processes. *SIAM J Sci Comput* 26:698–719. doi:<http://dx.doi.org/10.1137/S1064827503427741>
7. Eriksson S, Abbas Q, Nordström J (2011) A stable and conservative method for locally adapting the design order of finite difference schemes. *J Comput Phys* 230(11):4216–4231. doi:<http://dx.doi.org/10.1016/j.jcp.2010.11.020>
8. Gerritsen M, Olsson P (1996) Designing an efficient solution strategy for fluid flows. *J Comput Phys* 129(2):245–262. doi:[10.1006/jcph.1996.0248](https://doi.org/10.1006/jcph.1996.0248), <http://dx.doi.org/10.1006/jcph.1996.0248>
9. Gottlieb S, Shu CW (1998) Total variation diminishing runge-kutta schemes. *Math Comput* 67:73–85
10. Haas JF, Sturtevant B (1987) Interaction of weak shock waves with cylindrical and spherical gas inhomogeneities. *J Fluid Mech* 181:41–76. doi:[10.1017/S0022112087002003](https://doi.org/10.1017/S0022112087002003)

11. Harten A (1983) On the symmetric form of systems of conservation laws with entropy. *J Comput Phys* 49(1):151–164. doi:[10.1016/0021-9991\(83\)90118-3](https://doi.org/10.1016/0021-9991(83)90118-3), <http://www.sciencedirect.com/science/article/pii/0021999183901183>
12. Harten A, Lax PD, van Leer B (1983) On upstream differencing and Godunov-type schemes for hyperbolic conservation laws. *SIAM Rev* 25(1):35–61. <http://www.jstor.org/stable/2030019>
13. Kreiss HO, Scherer G (1974) Finite element and finite difference methods for hyperbolic partial differential equations. In: *Mathematical aspects of finite elements in partial differential equations*. Academic, New York, pp 179–183
14. Li H, Zhang D (2009) Efficient and accurate quantification of uncertainty for multiphase flow with the probabilistic collocation method. *SPE J* 14(4):665–679
15. Mattsson K, Nordström J (2004) Summation by parts operators for finite difference approximations of second derivatives. *J Comput Phys* 199(2):503–540. doi:[10.1016/j.jcp.2004.03.001](https://doi.org/10.1016/j.jcp.2004.03.001), <http://dx.doi.org/10.1016/j.jcp.2004.03.001>
16. Pettersson P, Iaccarino G, Nordström J (2009) Numerical analysis of the Burgers' equation in the presence of uncertainty. *J Comput Phys* 228:8394–8412. doi:[10.1016/j.jcp.2009.08.012](https://doi.org/10.1016/j.jcp.2009.08.012), <http://dl.acm.org/citation.cfm?id=1621150.1621394>
17. Pettersson P, Iaccarino G, Nordström J (2013) An intrusive hybrid method for discontinuous two-phase flow under uncertainty. *Comput Fluids* 86(0):228–239. doi:<http://dx.doi.org/10.1016/j.compfluid.2013.07.009>
18. Pettit CL, Beran PS (2006) Spectral and multiresolution Wiener expansions of oscillatory stochastic processes. *J Sound Vib* 294:752–779
19. Schwab C, Tokareva SA (2011) High order approximation of probabilistic shock profiles in hyperbolic conservation laws with uncertain initial data. Tech Rep 2011–53, ETH, Zürich
20. So KK, Chantramsi T, Hu XY, Witteveen JAS, Stemmer C, Iaccarino G, Adams NA (2010) Uncertainty analysis for shock-bubble interaction. In: *Proceedings of the 2010 summer program*. Center for Turbulence Research, Stanford University
21. Sod GA (1978) A survey of several finite difference methods for systems of nonlinear hyperbolic conservation laws. *J Comput Phys* 27(1):1–31. doi:[10.1016/0021-9991\(78\)90023-2](https://doi.org/10.1016/0021-9991(78)90023-2), <http://www.sciencedirect.com/science/article/pii/0021999178900232>
22. Strand B (1994) Summation by parts for finite difference approximations for d/dx . *J Comput Phys* 110(1):47–67. doi:<http://dx.doi.org/10.1006/jcph.1994.1005>
23. van Leer B (1979) Towards the ultimate conservative difference scheme. V – a second-order sequel to Godunov's method. *J Comput Phys* 32:101–136. doi:[10.1016/0021-9991\(79\)90145-1](https://doi.org/10.1016/0021-9991(79)90145-1)
24. Xiu D, Karniadakis GE (2002) The Wiener–Askey polynomial chaos for stochastic differential equations. *SIAM J Sci Comput* 24(2):619–644. doi:<http://dx.doi.org/10.1137/S1064827501387826>